Science of the Total Environment 722 (2020) 137934

Contents lists available at ScienceDirect

Science of the Total Environment

journal homepage: www.elsevier.com/locate/scitotenv

Comparison between idling and cruising gasoline vehicles in primary emissions and secondary organic aerosol formation during photochemical ageing

Yanli Zhang [a,b], Wei Deng [a], Qihou Hu [a,c], Zhenfeng Wu [a,d], Weiqiang Yang [a], Huina Zhang [a,d], Zhaoyi Wang [a], Zheng Fang [a], Ming Zhu [a,d], Sheng Li [a,d], Wei Song [a], Xiang Ding [a], Xinming Wang [a,b,d,*]

[a] State Key Laboratory of Organic Geochemistry and Guangdong Key Laboratory of Environmental Protection and Resources Utilization, Guangzhou Institute of Geochemistry, Chinese Academy of Sciences, Guangzhou 510640, China
[b] Center for Excellence in Regional Atmospheric Environment, Institute of Urban Environment, Chinese Academy of Sciences, Xiamen 361021, China
[c] Key Lab of Environmental Optics & Technology, Anhui Institute of Optics and Fine Mechanics, Chinese Academy of Sciences, Hefei 230031, China
[d] University of Chinese Academy of Sciences, Beijing 100049, China

HIGHLIGHTS

- Primary emissions and SOA formation from hot idling and cruising gasoline vehicle were compared.
- Emissions at idling and cruising varied greatly in the NMHC/NOx ratios and NMHC compositions.
- Aromatics could explain 30–64% of measured SOA at idling, but less than 15% of that at cruising.

GRAPHICAL ABSTRACT

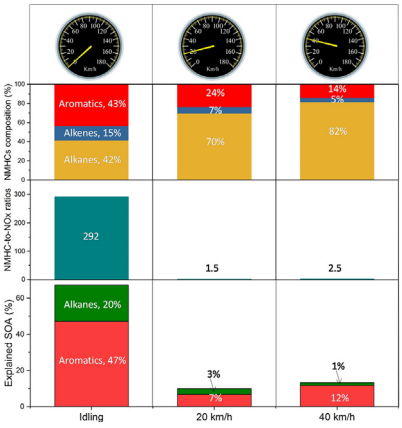

ARTICLE INFO

Article history:
Received 7 January 2020
Received in revised form 16 February 2020
Accepted 13 March 2020
Available online 14 March 2020

Editor: Jianmin Chen

Keywords:
Gasoline vehicle exhaust
Non-methane hydrocarbons
Secondary organic aerosol

ABSTRACT

Driving conditions are among the important factors determining gasoline vehicle emissions, yet their relation with exhaust-derived secondary pollutants is poorly understood. Here, we introduced exhaust from a gasoline vehicle under hot idling and cruising conditions into an indoor smog chamber by using a chassis dynamometer and investigated the formation of secondary organic aerosols (SOA) during photochemical ageing under light after characterizing the primary emission of non-methane hydrocarbons (NMHCs), nitrogen oxide (NO_x) and primary organic aerosol (POA) in the dark. When compared to emission factors (EFs) at idling, during cruising at 20 km h^{-1} or 40 km h^{-1}, the EFs of NMHCs decreased by more than an order of magnitude, while the EFs of NO_x were more than doubled, resulting in a large drop in the NMHC-to-NO_x ratios. The percentages of reactive alkenes and aromatic hydrocarbons also decreased from idling to cruising at 20 km h^{-1} to that at 40 km h^{-1}. The emission factor of benzene, a carcinogenic compound, decreased more than 10 times from ~0.35 g kg-fuel^{-1} at idling to ~0.03 g kg-fuel^{-1} during cruising. During photochemical ageing of exhaust, substantial SOA

* Corresponding author at: State key Laboratory of Organic Geochemistry, Guangzhou Institute of Geochemistry, Chinese Academy of Sciences, Guangzhou 510640, China.
E-mail address: wangxm@gig.ac.cn (X. Wang).

https://doi.org/10.1016/j.scitotenv.2020.137934

Chamber simulation
Photochemical ageing
China

was formed, and the SOA/POA ratios decreased from 52 to 92 at idling to 4–14 during cruising. Traditional aromatics could explain 30–64% of the measured SOA at idling but less than 15% of the measured SOA during cruising. Our results highlight that traffic congestion would greatly promote the emission of reactive volatile organic compounds and carcinogenic benzene from gasoline vehicles and also show that NMHCs as a target in gasoline vehicle emission tests cannot effectively represent the SOA and ozone formation potentials of the partially oxidized hydrocarbons from poorly functioning converters.

1. Introduction

Vehicle emissions are major anthropogenic sources of carbonaceous particulate matter, especially in urban areas, not only through direct emissions of primary organic aerosol (POA) and black carbon (BC), but also through forming secondary organic aerosols (SOA) from the oxidation of emitted gaseous aromatic and aliphatic hydrocarbons (Gentner et al., 2017; Odum et al., 1997; Pandis et al., 1992). Although both diesel and gasoline vehicles are responsible for emitting a complex mixture of unburned and partially burned hydrocarbons that act as precursors to SOA (Jathar et al., 2013), their relative importance in forming SOA is becoming a controversial issue (Gentner et al., 2017). While studies demonstrated that diesel exhausts are much more efficient in forming SOA than gasoline exhausts (Deng et al., 2017a; Gentner et al., 2017; Gordon et al., 2014), the number of gasoline vehicles overwhelmingly dominates that of diesel vehicles in many regions (Bahreini et al., 2012; CVEMAR, 2018). In addition, some recent studies suggested that gasoline emissions may overtake diesel emissions in forming SOA (Bahreini et al., 2012) or may produce more carbonaceous particulate matter than emissions from modern filter-equipped diesel vehicles (May et al., 2014; Platt et al., 2017). Therefore, gasoline exhaust cannot be exempt from aerosol loading, and its contribution to SOA formation is a timely issue that needs in-depth understanding of the precursors and formation mechanisms.

Being a major contributor to volatile organic compounds (VOCs) and nitrogen oxides (NO_x), which are both the most important ozone precursors in metropolitan regions, gasoline vehicle emissions have drawn sustained attention for decades, and great efforts have been made to characterize emissions by various techniques, such as on-board tests (Huo et al., 2012; Liu et al., 2009; Shen et al., 2014; Shorter et al., 2005; Wang et al., 2011; Yao et al., 2015), remote sensing (Bishop and Stedman, 1996; Guo et al., 2007), and tunnel tests (Hueglin et al., 2006; Jamriska et al., 2004; Zhang et al., 2015a, 2018). However, chamber simulations of SOA formation from atmospheric ageing of gasoline exhausts have only appeared very recently and are still quite limited. Earlier studies revealed that the total amount of SOA produced from the atmospheric oxidation of whole gasoline vapor or a surrogate mixture relevant for gasoline exhaust can be well explained by the contributions of the individual aromatic constituents (Odum et al., 1997; Kleindienst et al., 2002). However, while photochemical ageing of exhaust from gasoline vehicles at idling and during cold start exhibited similar results that SOA formation could be largely explained by aromatic hydrocarbons in the exhausts (Nordin et al., 2013; Liu et al., 2015), other chamber studies demonstrated that during a driving cycle on a chassis dynamometer, only a small part of SOA formed from gasoline vehicle exhaust could be accounted for by aromatic hydrocarbons (Gordon et al., 2014; Platt et al., 2013), and other unspeciated or lower volatility compounds such as intermediate volatility organic compounds (IVOCs) could contribute substantially to SOA formation. These studies suggested that the SOA formation potential of gasoline exhaust may be heavily influenced by driving conditions, and there is also concern if restricting NMHCs in gasoline exhaust would effectively reduce its potential to form secondary pollutants such as SOA.

As suggested by Platt et al. (2013), it is necessary to more closely simulate real-world driving conditions to understand gasoline vehicular emissions and photochemical ageing processes. However, it is a long-lasting challenge for available tests to represent real-world on-road vehicular emissions. For example, idling vehicles usually have a lower combustion temperature and efficiency than cruising vehicles, and there could be significant differences in the chemical compositions of exhausts. Unified driving cycles, which include idle, acceleration/deceleration and cruise conditions, may have a better representation of real-world vehicular emissions, and thus are widely adopted for vehicle emission tests. However, unified driving cycles in different nations or regions may vary in their ratios of idling, acceleration, deceleration and cruising conditions. In this way, studying gasoline vehicle emissions and their SOA formation potentials at different driving conditions is a fundamental task for a deep understanding of the relationship between driving conditions and SOA formation potentials.

In the present study, we started by comparing SOA formation potentials for exhausts from a Euro 4 gasoline car at idling to that when cruising. By using a chassis dynamometer, the exhausts from gasoline vehicles at idling or cruising speeds of 20 km h^{-1} and 40 km h^{-1} were respectively introduced into a 30 m^3 smog chamber. The exhausts were first characterized in the dark for primary emissions and were then photochemically aged with lights on to study the formation of SOA. The purpose is to provide information about the overall primary and secondary contributions to air pollutants by gasoline vehicles under different driving conditions and to explore the differences in the primary emissions and SOA formation between idling and cruising for gasoline vehicles.

2. Materials and methods

2.1. Experimental setup

Emission characterization and photochemical ageing experiments were conducted in a 30 m^3 (L × H × W, 5 m × 3 m × 2 m) fluorinated ethylene propylene (FEP 100, Type 200A; DuPont, USA) Teflon indoor smog chamber at the Guangzhou Institute of Geochemistry, Chinese Academy of Sciences (GIG-CAS). The detailed setup and facilities of the chamber can be found elsewhere (Deng et al., 2017a, 2017b, 2020; Fang et al., 2017; Liu et al., 2015, 2016; Wang et al., 2014). In brief, 135 black lamps (1.2 *m* long, 60 W Philips/10R BL, Royal Dutch Philips Electronics Ltd., the Netherlands) were used as the light source, providing a NO_2 photolysis rate of 0.25 min^{-1}. The temperature was maintained at about approximately 25 °C with an accuracy within ±1 °C, and the relative humidity (RH) was set to approximately 50% (Table 1). The temperature inside the chamber was controlled by three cooling units (total power 40 kW) and was monitored by nine temperature sensors. Humidification was achieved by vaporizing Milli-Q ultrapure water contained in a 0.5 L Florence flask and the water vapor was flushed with purified dry air into the FEP reactor.

According to the 2016 Annual Report of Beijing Traffic Development (2016 Annual Report of Beijing Traffic Development), the average driving speed during rush hours in Beijing is approximately 23.3 km h^{-1} in urban areas and 37.7 km h^{-1} on freeways. Therefore, driving speeds of 20 and 40 km h^{-1} were selected to represent the average driving speeds on urban roads and on freeways, respectively. An in-use China IV (which is identical to Euro 4) light-duty gasoline vehicle was used in this study. The vehicle is one with a port fuel injection engine and was

Table 1
Initial experiment conditions and emission factors of NMHCs and NO_x at different driving speeds.

Exp#	Speed (km h^{-1})	Temp (°C)	RH (%)	NMHCs (ppbv)	NO (ppbv)	NO_2 (ppbv)	NMHCs-NO_x ratios (v/v)	EF_{NMHCs} (g kg-fuel^{-1})	EF_{NOx} (mg kg-fuel^{-1})
1	Idling	25.0 ± 0.5	50.5 ± 2.0	3416	18.6	1.6	169	5.22	5.3
2	Idling	25.2 ± 0.5	48.3 ± 1.8	3868	6.6	2.7	415	4.62	4.7
3	20	25.2 ± 0.7	53.7 ± 2.9	239	305	9.8	0.8	0.15	50.6
4	20	25.0 ± 0.4	52.1 ± 1.4	213	95.3	6.8	2.1	0.17	14.8
5	40	25.4 ± 0.6	51.5 ± 2.5	505	101	6.8	4.7	0.45	18.6
6	40	25.3 ± 0.5	47.7 ± 1.6	175	681	14	0.3	0.23	206

fueled with Grade 93 gasoline, meeting the China IV gasoline fuel standard. PFI-equipped vehicles still dominate the vehicle composition in China. Because of the higher fuel efficiency of the GDI-equipped vehicles, the market share of GDI-equipped vehicles in sales in 2016 reached approximately 25% in China (Du et al., 2018). With an electric chassis dynamometer (FCDM-100, Foshan Analytical Instrument Co., Ltd., China) located just outside the GIG-CAS chamber, exhausts were generated by the gasoline vehicle run by an experienced driver at hot idling, and at driving speeds of 20 and 40 km h^{-1}. During the driving tests in this study, the average driving speeds were recorded as 19.7 ± 1.2 and 40.2 ± 1.5 km h^{-1}, respectively (Fig. S1).

2.2. Instrumentation

Instruments used to characterize and quantify the gas- and particulate-phase species are listed in Table S1 and the detailed descriptions of these instruments and data analysis can be found elsewhere (Wang et al., 2014). In brief, a high resolution time-of-flight aerosol mass spectrometer (HR-ToF-AMS, Aerodyne Research Inc., USA) was used to measure the particle compositions, including OA, nitrates (NO_3^-), ammonium (NH_4^+), and sulfate (SO_4^{2-}) (DeCarlo et al., 2006). Gas-phase contribution to the fragment m/z 44 (CO_2^+) signal was corrected with measured CO_2 concentrations. Ionization efficiency of the HR-ToF-AMS was calibrated using 300 nm monodisperse ammonium nitrate particles. Data analysis was performed with IGOR pro 6 (Wavemetrics, USA), SQUIRREL 1.51 and PIKA 1.1. Particle number concentration and size distribution were measured by a scanning mobility particle sizer (SMPS, model 3080 classifier) and condensation particle counter (CPC, model 3775). A sheath flow of 3.0 L min^{-1} and a sampling flow of 0.3 L min^{-1} were used for the SMPS measurements, allowing for a size scanning range of 14–760 nm within 255 s. The aerosol mass was corrected with the data from SMPS.

Volatile organic compounds (VOCs) were measured both on-line and off-line. A proton transfer reaction time-of-flight mass spectrometer (PTR-ToF-MS, Model 2000, Ionicon Analytik GmbH, Austria) with detection limits down to the ppt range was used to measure the real time concentrations of VOCs inside the reactor. The performance of the PTR-ToF-MS has been described in detail previously (Jordan et al., 2009). The ion source of H_3O^+ was used in this study. The decay curve of toluene measured by PTR-ToF-MS was used to derive the OH radical concentrations for every 2 min during each experiment. Meanwhile, off-line VOC samples were also collected by using 2-L stainless steel canisters once half an hour during each experiment. These canister samples were used for the determination of C_2-C_{12} NMHCs (Table S2), CO, and CO_2. All canister samples were analyzed by an Agilent 5973N gas chromatography mass-selective detector/flame ionization detector (GC-MSD/FID; Agilent Technologies, USA) coupled to a Preconcentrator (Model 7100, Entech Instruments Inc., USA). The analytical procedures have been detailed elsewhere (Zhang et al., 2012, 2013a, 2013b). Sixty-seven C_2-C_{12} NMHCs species were quantified for each sample. CO was analyzed using an Agilent 6980 gas chromatography with a flame ionization detector and a packed column (5A molecular sieve 60/80 mesh, 3 m × 1/8 in. (Zhang et al., 2012), and CO_2 was analyzed using a HP 4890D gas chromatograph (Yi et al., 2007). Trace gases concentrations of ozone, NO-NO_2-NO_x, and NH_3 were monitored using ozone analyzer (EC9810, Ecotech, Australia), NO_x monitor (EC9841T, Ecotech, Australia) and NH_3 analyzer (Model 911-0016, Los Gatos Research, USA), respectively.

2.3. Experimental procedure

Prior to each experiment, the Teflon chamber reaction bag was flushed with dry purified air which generated by an air purification system (Wang et al., 2014) to ensure that background concentrations of hydrocarbons, O_3, NO_x, and aerosol particles in the chamber reactor were all below the detection limits. Before the vehicle exhaust injection, the temperature inside the reactor was set and stabilized at ~25 °C.

Exhaust from the gasoline vehicle was injected into the smog chamber through a heated inlet system using a Dekati® ejector diluter (DI-1000, Dekati Ltd., Finland). For the idling tests, the vehicle was started and then run on-road for approximately 30 min to warm up its catalytic converter before the exhaust from the vehicle running at hot idling was introduced into the chamber; for tests at driving speeds of 20 km h^{-1} and 40 km h^{-1} on the chassis dynamometer, the exhaust was introduced into the chamber after the driving speeds were stabilized by an experienced driver. The injection time varied from 30 to 50 min based on the concentrations of VOCs and NO_x reached inside the reactor. The stainless steel lines used for exhaust injection were preheated to 100 °C to reduce the loss of VOCs and particles during the injection. A schematic of the experimental procedures, instruments, and sampling associated with the chamber can be found in Fig. 1. The emission factors were obtained by characterizing the pollutants emitted into the chamber before the lights were turned on (Fang et al., 2017).

To adjust the final NMHC-to-NO_x ratios inside the reactor to approximate the ambient conditions after the completion of exhaust injection and emission characterization in the dark, additional NO was added for the hot idling experiments, while additional propene instead was introduced for the experiments at driving speeds of 20 km h^{-1} and 40 km h^{-1} (Table 1). As propene is not supposed to contribute to the formation of SOA, it has been widely used to adjust the NMHC-to-NO_x ratios in previous smog chamber studies (Chirico et al., 2010; Kroll and Seinfeld, 2008; Platt et al., 2013). After the adjustment, the NMHC-to-NO_x (ppbv/ppbv) ratios in this study ranged from 1.5:1 to 17.6:1, which are comparable to those reported in urban areas or the values in previous chamber studies on gasoline vehicle exhausts (Clairotte et al., 2013). After the primary emitted pollutants inside the reactor were characterized under dark conditions, the lamps were turned on for 5 h of photochemical ageing. After that, the black lamps were turned off, and an additional 2–3 h of characterization for the formed SOA was performed to correct the particle wall loss.

2.4. Emission factors

Emission factor (EF) of each primary emission pollutant or production factor (PF) of a secondary pollutant could be calculated on a fuel basis (g kg-gasoline^{-1}):

$$\mathrm{EF\ (or\ PF)} = 1000 \times [\Delta P] \times \frac{1}{\left(\frac{[\Delta CO_2]}{MW_{CO_2}} + \frac{[CO]}{MW_{CO}} + \frac{[\Delta HCs]}{MW_{HCs}}\right)} \times \frac{\omega_C}{MW_C} \quad (1)$$

where [ΔP], [ΔCO_2], [ΔCO], and [ΔHCs] are the background corrected

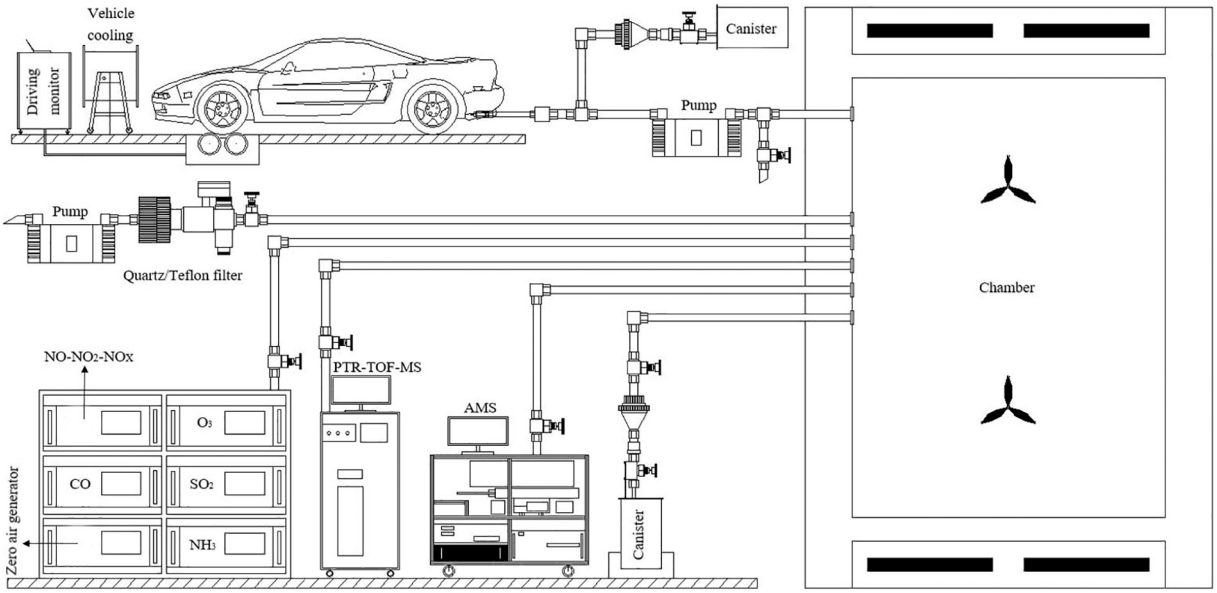

Fig. 1. Schematic map showing experiment setup and equipment connected to the indoor chamber.

concentrations of primary emission or secondary formation for pollutant P, CO_2, CO, and the C_2-C_{12} hydrocarbons determined by GC-MSD/FID system in the chamber reactor in μg m^{-3}; and MW_{CO2}, MW_{CO}, MW_{HCs}, and MW_C are molecular weights of CO_2, CO, HCs, and carbon. ω_C is the carbon intensity of the gasoline (Kirchstetter et al., 1999).

2.5. Wall loss corrections

Loss of particles onto the reactor walls may occur due to electrostatic forces, sedimentation and diffusion (McMurry and Grosjean, 1985). Detailed discussion about the wall loss corrections based on AMS data can be found in our previous studies (Deng et al., 2017a, 2017b, 2020; Fang et al., 2017; Liu et al., 2015, 2016; Wang et al., 2014). The wall loss rate constant was determined separately for each experiment by fitting the SMPS and AMS data with first-order kinetics when UV lamps were switched off. By applying this rate to the entire experiment, we use the same method as Pathak et al. (2007) to correct the wall loss of the particles. The impact of the nucleation event on wall loss is considered to be negligible as less than 3% of the particle mass is in the nucleation-mode 20 min after the start of photochemical ageing for all experiments in this study.

3. Results and discussions

3.1. Primary emissions of gaseous pollutants

One significant change in the primary emissions is that the NMHC-to-NO_x ratios (v/v) decreased from 169 and 415 at idling to 0.76 and 2.1, respectively, at the driving speed of 20 km h^{-1}, and to 0.25 and 4.7, respectively, at the driving speed of 40 km h^{-1} (Table 1). The EFs of total NMHCs decreased more than ten times from approximately 5.0 g kg-fuel^{-1} at idling to less than 0.5 g kg-fuel^{-1} at 20 km h^{-1} or at 40 km h^{-1}. Instead, the EFs of NO_x increased from ~5.0 mg kg-fuel^{-1} at idling to more than 10 mg kg-fuel^{-1} at 20 km h^{-1} or at 40 km h^{-1} (Table 1). The increasing trend of EFs of NOx with increased driving speeds is consistent with previous studies based on both tunnel tests (Martins et al., 2006) and chassis dynamometer tests (Yang et al., 2018).

Another significant change in the primary emissions was the composition of NMHCs. As shown in Fig. 2, aromatics accounted for the largest fraction (43%) of NMHCs at idling. However, the fractions of aromatics decreased to 24% at 20 km h^{-1} and further to 14% at 40 km h^{-1}. Similarly, the percentages of alkenes decreased from 15% at idling to 7% at 20 km h^{-1} and to only 4% at 40 km h^{-1}. In contrast, alkanes, including normal alkanes, branched alkanes and cycloalkanes, shared a fraction (42%) nearly the same as that of aromatics at idling, but their shares increased to 70% at 20 km h^{-1}, and further to 82% at 40 km h^{-1}, nearly double those at idling. The drop in more reactive unsaturated aromatics and alkenes and the increase in less reactive alkanes at a driving speed of 20 km h^{-1} are similar to the results for private gasoline cars at different driving speeds observed by Guo et al. (2011), in which the percentages of alkanes increased from 40% at idling to 54% at 25 km h^{-1} and 57% at 70 km h^{-1}, while those of aromatics decreased from 32% at idling to 29% at 25 km h^{-1} and 19% at 70 km h^{-1}. Aromatics, as an important group of anthropogenic VOCs that contribute to SOA formation (de Gouw et al., 2008; Ding et al., 2012), had an average emission factor of 2.7 g kg-fuel^{-1} at idling, 0.04 g kg-fuel^{-1} at 20 km h^{-1} and 0.05 g kg-fuel^{-1} at 40 km h^{-1}.These differences in the primary emissions between driving and idling also agreed with the results from engine experiments (Kean et al., 2003; Wang et al., 2013). Compared to conditions at idling, changed fuel/air ratios and higher burning temperatures under driving conditions would benefit more complete burning

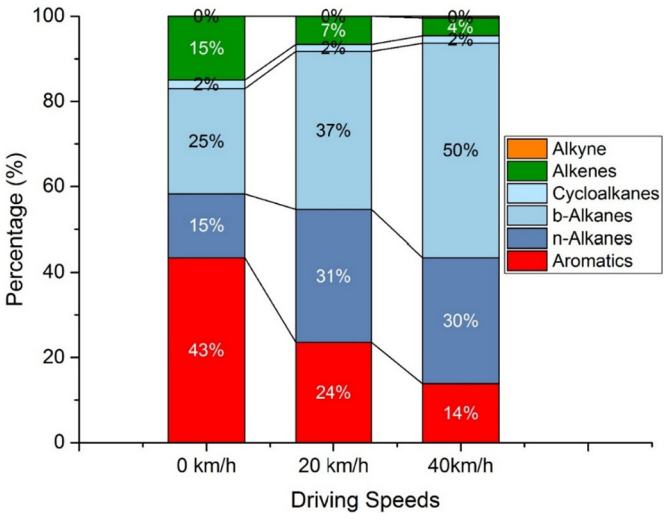

Fig. 2. Compositions of NMHCs determined offline by canister sampling at different driving conditions.

of fuels, leading to lower emissions of NHMCs and increased yields of NO_x.

3.2. Primary emissions and secondary productions of OA

Obviously new particle formation was observed during all experiments (Fig. S2). In the start, particle number concentrations of less than 120 cm^{-3} were observed in all experiments. They increased rapidly to about 6.8E+05 cm^{-3} at idling with a maximum particle density diameter at ~40 nm, but to less than 3.6E+04 cm^{-3} at the cruising experiments with the maximum particle density diameter at ~110 nm. The above drastic changes in primary NMHC-to-NO_x ratios as well as in EFs and compositions of VOCs would inevitably influence the potential formation of secondary products, including SOA (Ng et al., 2007). As shown in Fig. 3, the average EF of POA at idling was 0.32 ± 0.02 mg kg-$fuel^{-1}$, much lower than that of 1.4 ± 0.7 mg kg-$fuel^{-1}$ at 20 km h^{-1} and 1.5 ± 0.8 mg kg-$fuel^{-1}$ at 40 km h^{-1}. The average PF of SOA under idling conditions (23.4 ± 5.4 mg kg-$fuel^{-1}$) was higher than that of 15.2 ± 2.1 mg kg-$fuel^{-1}$ at 20 km h^{-1}, and much higher than that of 9.1 ± 0.5 mg kg-$fuel^{-1}$ at 40 km h^{-1}. As a result, the SOA/POA ratios decreased from 52 and 92 at idling to 4–14 during cruising.

According to field observations downwind of an urban area by de Gouw et al. (2005), SOA production continues for approximately 48 h at an OH level of 3×10^6 molecules cm^{-3}. Therefore, five-hour photochemical ageing with OH exposure of $(1.4–4.7) \times 10^6$ molecules cm^{-3} (Table 2) in this study might underestimate the final SOA production. The average EF of POA under idling conditions in this study in 2016 is comparable with that of 0.34 ± 0.02 mg kg-$fuel^{-1}$ in 2013 reported by Liu et al. (2015) for the same test vehicle, while the average PF of SOA at idling reported by Liu et al. (2015) was 1.4 times that in this study. When compared to previous studies on exhaust from idling gasoline cars, the average PF of SOA (0.023 g kg-$fuel^{-1}$) in this study lies in the middle of the range, i.e., 0.005–0.09 g kg-$fuel^{-1}$, reported by Nordin et al. (2013) (EURO-2 to EURO-4 gasoline vehicles), and 0.001–0.044 g kg-$fuel^{-1}$, reported by Liu et al. (2015) (EURO-1 to EURO-4 gasoline vehicles). The EFs of POA at idling and cruising in this study were significantly lower than those reported by Platt et al. (2013), i.e., $(1.97–2.45) \times 10^{-2}$ g kg-$fuel^{-1}$, for a Euro-5 gasoline vehicle operated under a New European Driving Cycle (NEDC) condition, or the range reported by Gordon et al. (2014), i.e., 7×10^{-3} g kg-$fuel^{-1}$ to 1×10^{-2} g kg-$fuel^{-1}$, for 15 light-duty gasoline vehicles under the Unified Cycle (UC) conditions in California. Accordingly, the PFs of SOA in this study were also obviously lower than those of 0.344–0.347 g kg-$fuel^{-1}$ in Platt et al. (2013) or 0.02–0.13 g kg-$fuel^{-1}$ in Gordon et al.

Table 2
POA and photochemically formed SOA at different driving speeds.

Exp. #	Driving speed (km h^{-1})	OH exposure ($\times 10^6$ molecules cm^{-3})	POA (μg m^{-3})	SOA (μg m^{-3})	SOA/POA
1	IDLING	3.13	0.74	68.2	92.2
2	IDLING	4.19	0.92	48.2	52.4
3	20	1.41	8.05	94.8	11.8
4	20	2.6	3.28	26.2	8.0
5	40	2.38	2.47	35	14.2
6	40	4.66	4.76	18.1	3.8

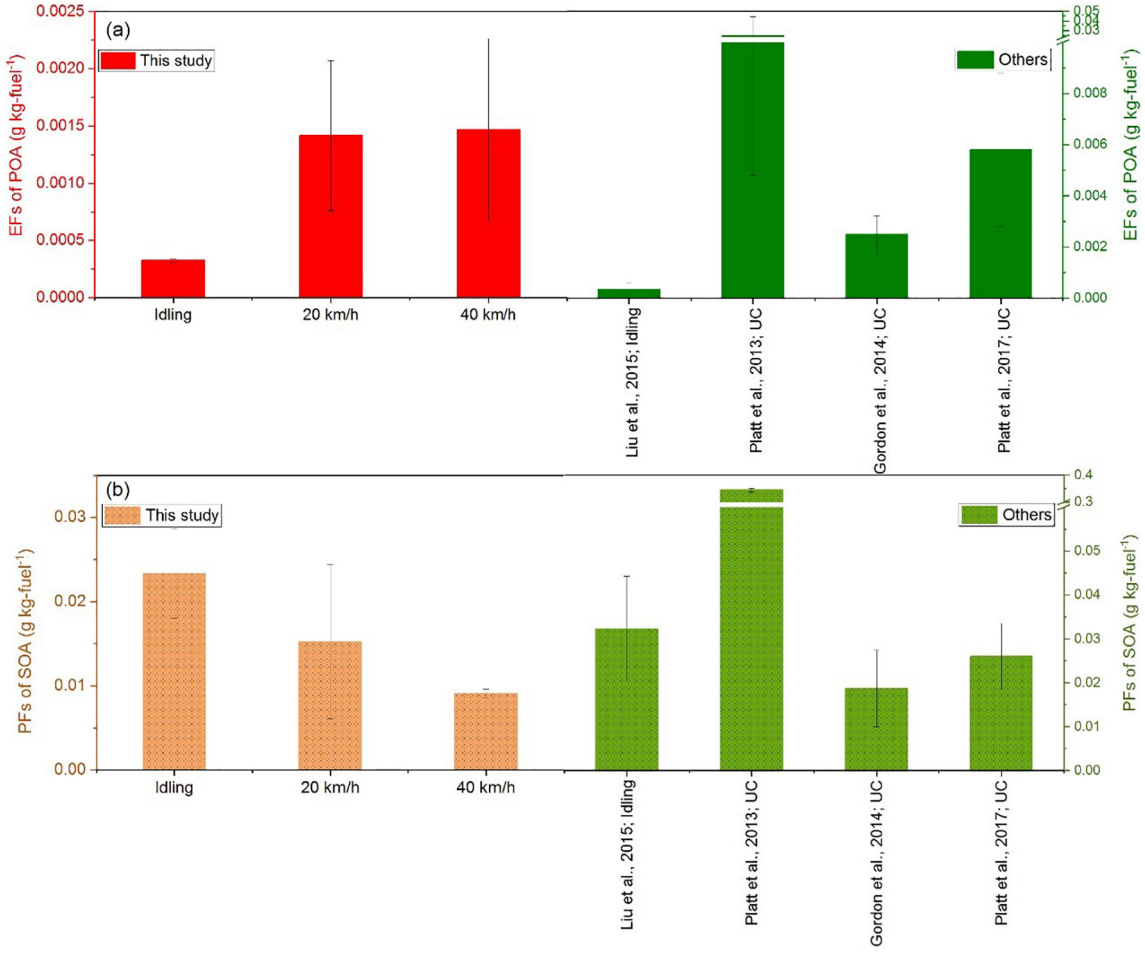

Fig. 3. Emission factors (EFs) of POA (a) and production factors (PFs) of SOA (b) at idling, 20 km h^{-1} and 40 km h^{-1} in this study. The results from other studies are also showed in the figure.

(2014). Ratios of POA/SOA with a range of 4–92 in this study, were in the middle of the values (1–259) in previous studies (Gordon et al., 2014; Liu et al., 2015; Nordin et al., 2013; Platt et al., 2013). The EFs of POA or PFs of SOA under NEDC or UC conditions were reasonably higher since more emissions occur during accelerating or decelerating than during driving at stabilized speeds (Tong et al., 2000).

The EFs of POA or PFs of SOA for exhaust from gasoline vehicles were extremely low when compared with those reported for exhaust from diesel vehicles, such as the EFs of POA ranging 0.05–0.91 g kg-fuel^{-1} for idling and driving diesel vehicles (Chirico et al., 2010; Deng et al., 2017a; Gordon et al., 2014), the PFs of SOA ranging 0.5–1.8 g kg-fuel^{-1} for idling diesel vehicles (Chirico et al., 2010; Deng et al., 2017a), or an SOA PF of 0.47 g kg-fuel^{-1} for diesel vehicles under driving cycles Gordon et al. (2014).

3.3. SOA production explained by precursors

With the consumption of typical traditional precursors, such as benzene, toluene, C_8-AHs and C_9-AHs, as observed by PTR-ToF-MS online, their contributions to SOA could be estimated as:

$$SOA_{estimated} = \sum_i \Delta M_i \times Y_i \quad (2)$$

where ΔM_i is the amount of precursor species i that was consumed during photochemical ageing, and Y_i is the SOA yield for precursor species i, which could be approximated with a semiempirical two-product model based on absorptive gas-particle partitioning (Borrás and Tortajada-Genaro, 2012; Odum et al., 1996, 1997; Ng et al., 2007; Shakya and Griffin, 2010). Fig. 4 shows the predicted SOA derived from NMHCs including benzene, toluene, C_8-AHs, C_9-AHs, and naphthalene against the total measured SOA. At idling, 30–64% of the measured SOA could be explained by these aromatics which are among the most important anthropogenic SOA precursors. However, for tests under cruising conditions, larger gaps between predicted and measured SOA were observed. The predicted SOA formed from these aromatics could only explain less than 15% of the measured SOA. The predicted SOA from the aromatics were 2–12% at 20 km h^{-1} and 10–14% at 40 km h^{-1}. At idling, the result is consistent with that from previous studies on photochemical ageing of exhaust from idling gasoline vehicles: these aromatics could explain 51–90% of the formed SOA in the study by Liu et al. (2015) and up to 60% of formed SOA in the study by Nordin et al. (2013). For exhausts from gasoline cars under the NEDC condition (Platt et al., 2013), the predicted SOA by aromatics and naphthalene could reach up to 20% of the measured SOA. This percentage between the idling and driving situations is reasonable since emissions of aromatics under standard driving cycles might also lie between those at idling and at cruising. Previous studies illustrated that C_7-C_{12} alkanes could also contribute to SOA formation (Lim and Ziemann, 2009a, 2009b; Loza et al., 2014). As estimated based on eq. (2), alkanes could contribute 19–21% of the measured SOA at idling but only 0.1–6% at 20 km h^{-1} and 0.2–3% at 40 km h^{-1}. Additionally, aromatics and alkanes together could explain 49–86% of the formed SOA at idling (Fig. 4), but could still not explain the formed SOA at cruising. They could only account for 2–18% and 13–14% of formed SOA at 20 km h^{-1} and 40 km h^{-1}, respectively. This large gap between the measured SOA and SOA predicted from traditional precursors suggests that there were unknown precursors that might also contribute substantially to SOA formation, since even from carbon balance, it is impossible for the traditional precursors to afford the SOA formed. Gordon et al. (2014) indicated that approximately 30% of the non-methane hydrocarbons from vehicle exhaust could not be speciated and that they may contribute to SOA formation. Zhao et al. (2014a, 2014b, 2015, 2016) measured IVOCs in vehicle exhausts. They estimated that for gasoline vehicles although IVOCs were only approximately 4% of NMHCs in primary emissions, they could contribute as much as or even more SOA than the single-ring aromatics.

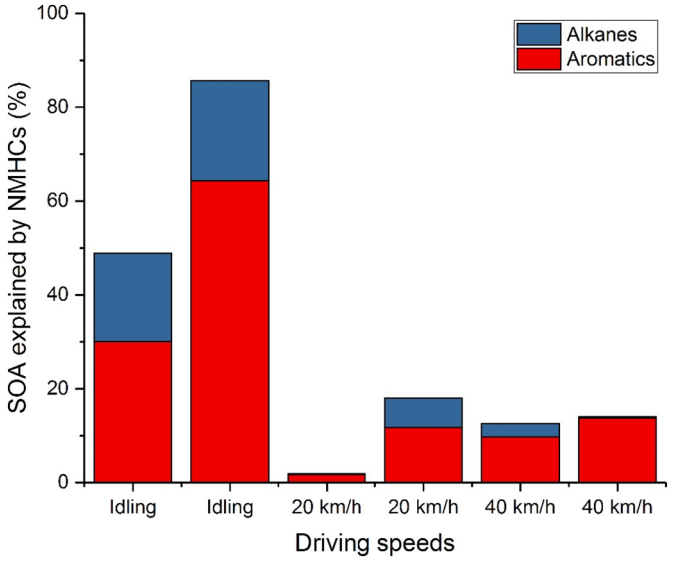

Fig. 4. Percentages of measured SOA as predicted by the contribution of aromatic hydrocarbons and alkanes.

4. Conclusions

With the rapid increase in vehicle numbers, traffic congestion has become a big problem in many urban areas. In Hong Kong, for example, vehicle number increased by 30% from 2003 to 2013, and the average car travel speed in urban areas dropped by approximately 11% during the decade. In China's capital city Beijing, the daily road traffic congestion hours increased from 1.9 h in 2014 to 3 h in 2015, and the annual average driving speeds across its whole road network decreased from 28.1 km h^{-1} in 2014 to 25.1 km h^{-1} in 2015 (2016 Annual Report of Beijing Traffic Development). Based on our study, a gasoline vehicle cruising at 40 km h^{-1} had a more than 50% lower SOA production factor (9.1 mg kg-fuel^{-1}) when compared to that (23 mg kg-fuel^{-1}) for a hot idling vehicle. A rough estimation of ozone formation potential with the maximum incremental reactivity method (Carter, 2009) (Fig. S3) also revealed that the total OFPs of all VOC species in exhausts dropped over 30 times from approximately 22 g kg-fuel^{-1} at idling to about 0.5 g kg-fuel^{-1} when cruising at 40 km h^{-1}. Therefore, more hot idling hours induced by traffic congestion means more emissions of reactive aromatics and alkenes, and thereby more production of SOA as well as ozone. This implies that reducing traffic congestion would not only improve transportation efficiency, but also benefit alleviating severe $PM_{2.5}$ and ozone pollution through reducing vehicle emissions of precursors for SOA and ozone.

It is worth noting that cruising gasoline vehicles had much lower emissions of hazardous air pollutants such as benzene than idling vehicles. Previous studies have revealed a higher cancer risk of benzene in China's developed regions (Zhang et al., 2015b, 2016a, 2016b) with gasoline exhaust as one of its major sources in urban (Wang et al. 2002; Zhang et al., 2012, 2013a, 2018). In our study, the emission factor of benzene decreased more than ten times from ~0.35 g kg-fuel^{-1} at idling to ~0.03 g kg-fuel^{-1} during cruising. Therefore, reducing traffic congestion can also lower people's health risk when exposed to traffic-related microenvironments. Another important implication from our study is that, although NMHCs are targeted during gasoline vehicle emission tests, they cannot reflect the exhausts' potential to form SOA or even ozone.

CRediT authorship contribution statement

Yanli Zhang: Conceptualization, Formal analysis, Writing - original draft, Investigation. **Wei Deng:** Investigation. **Qihou Hu:** Investigation.

Zhenfeng Wu: Formal analysis. **Weiqiang Yang:** Formal analysis. **Huina Zhang:** Formal analysis. **Zhaoyi Wang:** Investigation. **Zheng Fang:** Investigation. **Ming Zhu:** Investigation. **Sheng Li:** Investigation. **Wei Song:** Project administration. **Xiang Ding:** Project administration. **Xinming Wang:** Conceptualization, Formal analysis, Writing - original draft.

Declaration of competing interest

The authors declare that they have no known competing financial interests or personal relationships that could have appeared to influence the work reported in this paper.

Acknowledgements

This work was supported by the National Key Research and Development Program (2017YFC0212802/2016YFC0202204), the Chinese Academy of Sciences (Grant No. QYZDJ-SSW-DQC032/XDA23020301/XDA23010303), the National Natural Science Foundation of China (Grant No. 41673116/41530641/41571130031), Youth Innovation Promotion Association of the Chinese Academy of Sciences (2017406), and Guangdong Foundation for Program of Science and Technology Research (Grant No. 2017B030314057).

Appendix A. Supplementary data

Supplementary data to this article can be found online at https://doi.org/10.1016/j.scitotenv.2020.137934.

References

2016 Annual Report of Beijing Traffic Development, 2016. Beijing Transport Institute (Assessed August 3, 2018).

Bahreini, R., Middlebrook, A.M., de Gouw, J.A., Warneke, C., Trainer, M., Brock, C.A., Stark, H., Brown, S.S., Dube, W.P., Gilman, J.B., Hall, K., Holloway, J.S., Kuster, W.C., Perring, A.E., Prevot, A.S.H., Schwarz, J.P., Spackman, J.R., Szidat, S., Wagner, N.L., Weber, R.J., Zotter, P., Parrish, D.D., 2012. Gasoline emissions dominate over diesel in formation of secondary organic aerosol mass. Geophys. Res. Lett. 39, L06805. https://doi.org/10.1029/2011GL050718.

Bishop, G.A., Stedman, D.H., 1996. Measuring the emissions of passing cars. Accounts Chem. Res. 29, 489–495.

Borrás, E., Tortajada-Genaro, L.A., 2012. Secondary organic aerosol formation from the photo-oxidation of benzene. Atmos. Environ. 47, 154–163.

Carter, W.P.L., 2009. Update maximum incremental reactivity scale and hydrocarbon bin reactivities for regulatory application. California Air Resources Board (Contract 07-339).

China Vehicle Environmental Management Annual Report, 2018. Ministry of Ecology and Environment of the People's Republic of China. http://www.mee.gov.cn/xxgk2018/xxgk/xxgk15/201806/t20180601_630215.html.

Chirico, R., DeCarlo, P.F., Heringa, M.F., Tritscher, T., Richter, R., Prevot, A.S.H., Dommen, J., Weingartner, E., Wehrle, G., Gysel, M., Laborde, M., Baltensperger, U., 2010. Impact of after treatment devices on primary emissions and secondary organic aerosol formation potential from in-use diesel vehicles: results from smog chamber experiments. Atmos. Chem. Phys. 10 (23), 11545–11563.

Clairotte, M., Adam, T.W., Zardini, A.A., Manfredi, U., Martini, G., Krasenbrink, A., Vicet, A., Tournie, E., Astorga, C., 2013. Effects of low temperature on the cold start gaseous emissions from light duty vehicles fuelled by ethanol-blended gasoline. Appl. Energy 102, 44–54.

DeCarlo, P.F., Kimmel, J.R., Trimborn, A., Northway, M.J., Jayne, J.T., Aiken, A.C., Gonin, M., Fuhrer, K., Horvath, T., Docherty, K.S., Worsnop, D.R., Jimenez, J.L., 2006. Field-deployable, high-resolution, time-of-flight aerosol mass spectrometer. Anal. Chem. 78 (24), 8281–8289.

Deng, W., Hu, Q., Liu, T., Wang, X., Zhang, Y., Song, W., Sun, Y., Bi, X., Yu, J., Yang, W., Huang, X., Zhang, Z., Huang, Z., He, Q., Mellouki, A., George, C., 2017a. Primary particulate emissions and secondary organic aerosol (SOA) formation from idling diesel vehicle exhaust in China. Sci. Total Environ. 593-594, 462–469.

Deng, W., Fang, Z., Wang, Z., Zhu, M., Zhang, Y., Tang, M., Song, W., Lowther, S., Huang, Z., Jones, K., Peng, P.A., Wang, X., 2020. Primary emissions and secondary organic aerosol formation from in-use diesel vehicle exhaust: comparison between idling and cruise mode. Sci. Total Environ. 699, 134357.

Deng, W., Liu, T.Y., Zhang, Y.L., Situ, S.P., Hu, Q.H., He, Q.F., Zhang, Z., Lu, S.J., Bi, X.H., Wang, X.M., Boreave, A., George, C., Ding, X., Wang, X.M., 2017b. Secondary organic aerosol formation from photo-oxidation of toluene with NOx and SO_2: chamber simulation with purified air versus urban ambient air as matrix. Atmos. Environ. 150, 67–76.

Ding, X., Wang, X.-M., Gao, B., Fu, X.-X., He, Q.-F., Zhao, X.-Y., Yu, J.-Z., Zheng, M., 2012. Tracer-based estimation of secondary organic carbon in the Pearl River Delta, south China. J. Geophys. Res.-Atmos. 117, D05313. https://doi.org/10.1029/2011jd016596.

Du, Z., Hu, M., Peng, J., Zhang, W., Zheng, J., Gu, F., Qin, Y., Yang, Y., Li, M., Wu, Y., Shao, M., Shuai, S., 2018. Comparison of primary aerosol emission and secondary aerosol formation from gasoline direct injection and port fuel injection vehicles. Atmos. Chem. Phys. 18 (12), 9011–9023.

Fang, Z., Deng, W., Zhang, Y.L., Ding, X., Tang, M.J., Liu, T.Y., Hu, Q.H., Zhu, M., Wang, Z.Y., Yang, W.Q., Huang, Z.H., Song, W., Bi, X.H., Chen, J.M., Sun, Y.L., George, C., Wang, X.M., 2017. Open burning of rice, corn and wheat straws: primary emissions, photochemical aging, and secondary organic aerosol formation. Atmos. Chem. Phys. 17 (24), 14821–14839.

Gentner, D.R., Jathar, S.H., Gordon, T.D., Bahreini, R., Day, D.A., El Haddad, I., Hayes, P.L., Pieber, S.M., Platt, S.M., de Gouw, J., Goldstein, A.H., Harley, R.A., Jimenez, J.L., Prevot, A.S.H., Robinson, A.L., 2017. Review of urban secondary organic aerosol formation from gasoline and diesel motor vehicle emissions. Environ. Sci. Technol. 51 (3), 1074–1093.

Gordon, T.D., Presto, A.A., May, A.A., Nguyen, N.T., Lipsky, E.M., Donahue, N.M., Gutierrez, A., Zhang, M., Maddox, C., Rieger, P., Chattopadhyay, S., Maldonado, H., Maricq, M.M., Robinson, A.L., 2014. Secondary organic aerosol formation exceeds primary particulate matter emissions for light-duty gasoline vehicles. Atmos. Chem. Phys. 14 (9), 4661–4678.

de Gouw, J.A., Middlebrook, A.M., Warneke, C., Goldan, P.D., Kuster, W.C., Roberts, J.M., Fehsenfeld, F.C., Worsnop, D.R., Canagaratna, M.R., Pszenny, A.A.P., Keene, W.C., Marchewka, M., Bertman, S.B., Bates, T.S., 2005. Budget of organic carbon in a polluted atmosphere: results from the New England Air Quality Study in 2002. J. Geophys. Res.-Atmos. 110, D16305. https://doi.org/10.1029/2004jd005623.

de Gouw, J.A., Brock, C.A., Atlas, E.L., Bates, T.S., Fehsenfeld, F.C., Goldan, P.D., Holloway, J.S., Kuster, W.C., Lerner, B.M., Matthew, B.M., Middlebrook, A.M., Onasch, T.B., Peltier, R.E., Quinn, P.K., Senff, C.J., Stohl, A., Sullivan, A.P., Trainer, M., Warneke, C., Weber, R.J., Williams, E.J., 2008. Sources of particulate matter in the northeastern United States in summer: 1. Direct emissions and secondary formation of organic matter in urban plumes. J. Geophys. Res.-Atmos. 113, D08301. https://doi.org/10.1029/2007jd009243.

Guo, H., Zhang, Q.Y., Shi, Y., Wang, D.H., 2007. Evaluation of the International Vehicle Emission (IVE) model with on-road remote sensing measurements. J. Environ. Sci. 19 (7), 818–826.

Guo, H., Zou, S.C., Tsai, W.Y., Chan, L.Y., Blake, D.R., 2011. Emission characteristics of nonmethane hydrocarbons from private cars and taxis at different driving speeds in Hong Kong. Atmos. Environ. 45 (16), 2711–2721.

Hueglin, C., Buchmann, B., Weber, R., 2006. Long-term observation of real-world road traffic emission factors on a motorway in Switzerland. Atmos. Environ. 40, 3696–3709.

Huo, H., Yao, Z., Zhang, Y., Shen, X., Zhang, Q., Ding, Y., He, K., 2012. On-board measurements of emissions from light-duty gasoline vehicles in three mega-cities of China. Atmos. Environ. 49, 371–377.

Jamriska, M., Morawska, L., Thomas, S., He, C., 2004. Diesel bus emissions measured in a tunnel study. Environ. Sci. Technol. 38, 6701–6709.

Jathar, S.H., Miracolo, M.A., Tkacik, D.S., Donahue, N.M., Adams, P.J., Robinson, A.L., 2013. Secondary organic aerosol formation from photo-oxidation of unburned fuel: experimental results and implications for aerosol formation from combustion emissions. Environ. Sci. Technol. 47 (22), 12886–12893.

Jordan, A., Haidacher, S., Hanel, G., Hartungen, E., Maerk, L., Seehauser, H., Schottkowsky, R., Sulzer, P., Maerk, T.D., 2009. A high resolution and high sensitivity proton-transfer-reaction time-of-flight mass spectrometer (PTR-TOF-MS). Int. J. Mass Spectrom. 286 (2–3), 122–128.

Kean, A.J., Harley, R.A., Kendall, G.R., 2003. Effects of vehicle speed and engine load on motor vehicle emissions. Environ. Sci. Technol. 37 (17), 3739–3746.

Kirchstetter, T.W., Harley, R.A., Kreisberg, N.M., Stolzenburg, M.R., Hering, S.V., 1999. On-road measurement of fine particle and nitrogen oxide emissions from light- and heavy-duty motor vehicles. Atmos. Environ. 33 (18), 2955–2968.

Kleindienst, T.E., Corse, E.W., Li, W., McIver, C.D., Conver, T.S., Edney, E.O., Driscoll, D.J., Speer, R.E., Weathers, W.S., Tejada, S.B., 2002. Secondary organic aerosol formation from the irradiation of simulated automobile exhaust. J. Air & Waste Manage. Assoc. 52 (3), 259–272.

Kroll, J.H., Seinfeld, J.H., 2008. Chemistry of secondary organic aerosol: formation and evolution of low-volatility organics in the atmosphere. Atmos. Environ. 42 (16), 3593–3624.

Lim, Y.B., Ziemann, P.J., 2009a. Chemistry of secondary organic aerosol formation from OH radical-initiated reactions of linear, branched, and cyclic alkanes in the presence of NOx. Aerosol Sci. Technol. 43 (6), 604–619.

Lim, Y.B., Ziemann, P.J., 2009b. Effects of molecular structure on aerosol yields from OH radical-initiated reactions of linear, branched, and cyclic alkanes in the presence of NOx. Environ. Sci. Technol. 43 (7), 2328–2334.

Liu, H., He, K., Lents, J.M., Wang, Q., Tolvett, S., 2009. Characteristics of diesel truck emission in China based on portable emissions measurement systems. Environ. Sci. Technol. 43 (24), 9507–9511.

Liu, T., Wang, X., Deng, W., Hu, Q., Ding, X., Zhang, Y., He, Q., Zhang, Z., Lu, S., Bi, X., Chen, J., Yu, J., 2015. Secondary organic aerosol formation from photochemical aging of light-duty gasoline vehicle exhausts in a smog chamber. Atmos. Chem. Phys. 15 (15), 9049–9062.

Liu, T., Wang, X., Hu, Q., Deng, W., Zhang, Y., Ding, X., Fu, X., Bernard, F., Zhang, Z., Lu, S., He, Q., Bi, X., Chen, J., Sun, Y., Yu, J., Peng, P., Sheng, G., 2016. Fu, J. Formation of secondary aerosols from gasoline vehicle exhaust when mixing with SO_2. Atmos. Chem. Phys. 16 (2), 675–689.

Loza, C.L., Craven, J.S., Yee, L.D., Coggon, M.M., Schwantes, R.H., Shiraiwa, M., Zhang, X., Schilling, K.A., Ng, N.L., Canagaratna, M.R., Ziemann, P.J., Flagan, R.C., Seinfeld, J.H.,

2014. Secondary organic aerosol yields of 12-carbon alkanes. Atmos. Chem. Phys. 14 (3), 1423–1439.
Martins, L.D., Andrade, M.F., D Freitas, E., Pretto, A., Gatti, L.V., Albuquerque, E.L., Tomaz, E., Guardani, M.L., Martins, M.H.R.B., Junior, O.M.A., 2006. Emission factors for gas-powered vehicles traveling through road tunnels in Sao Paulo, Brazil. Environ. Sci. Technol. 40 (21), 6722–6729.
May, A.A., Nguyen, N.T., Presto, A.A., Gordon, T.D., Lipsky, E.M., Karve, M., Gutierrez, A., Robertson, W.H., Zhang, M., Brandow, C., Chang, O., Chen, S., Cicero-Fernandez, P., Dinkins, L., Fuentes, M., Huang, S.-M., Ling, R., Long, J., Maddox, C., Massetti, J., McCauley, E., Miguel, A., Na, K., Ong, R., Pang, Y., Rieger, P., Sax, T., Tin, T., Thu, V., Chattopadhyay, S., Maldonado, H., Maricq, M.M., Robinson, A.L., 2014. Gas- and particle-phase primary emissions from in-use, on-road gasoline and diesel vehicles. Atmos. Environ. 88, 247–260.
McMurry, P.H., Grosjean, D., 1985. Gas and aerosol wall losses in Teflon film smog chambers. Environ. Sci. Technol. 19 (12), 1176–1182.
Ng, N.L., Kroll, J.H., Chan, A.W.H., Chhabra, P.S., Flagan, R.C., Seinfeld, J.H., 2007. Secondary organic aerosol formation from m-xylene, toluene, and benzene. Atmos. Chem. Phys. 7 (14), 3909–3922.
Nordin, E.Z., Eriksson, A.C., Roldin, P., Nilsson, P.T., Carlsson, J.E., Kajos, M.K., Hellen, H., Wittbom, C., Rissler, J., Londahl, J., Swietlicki, E., Svenningsson, B., Bohgard, M., Kulmala, M., Hallquist, M., Pagels, J.H., 2013. Secondary organic aerosol formation from idling gasoline passenger vehicle emissions investigated in a smog chamber. Atmos. Chem. Phys. 13 (12), 6101–6116.
Odum, J.R., Hoffmann, T., Bowman, F., Collins, D., Flagan, R.C., Seinfeld, J.H., 1996. Gas/particle partitioning and secondary organic aerosol yields. Environ. Sci. Technol. 30 (8), 2580–2585.
Odum, J.R., Jungkamp, T.P.W., Griffin, R.J., Flagan, R.C., Seinfeld, J.H., 1997. The atmospheric aerosol-forming potential of whole gasoline vapor. Science 276 (5309), 96–99.
Pandis, S.N., Harley, R.A., Cass, G.R., Seinfeld, J.H., 1992. Secondary organic aerosol formation and transport. Atmos. Environ. Part a-General Topics 26 (13), 2269–2282.
Pathak, R.K., Stanier, C.O., Donahue, N.M., Pandis, S.N., 2007. Ozonolysis of alpha-pinene at atmospherically relevant concentrations: temperature dependence of aerosol mass fractions (yields). J. Geophys. Res.-Atmos. 112, D03201. https://doi.org/10.1029/2006jd007436.
Platt, S.M., El Haddad, I., Zardini, A.A., Clairotte, M., Astorga, C., Wolf, R., Slowik, J.G., Temime-Roussel, B., Marchand, N., Jezek, I., Drinovec, L., Mocnik, G., Moehler, O., Richter, R., Barmet, P., Bianchi, F., Baltensperger, U., Prevot, A.S.H., 2013. Secondary organic aerosol formation from gasoline vehicle emissions in a new mobile environmental reaction chamber. Atmos. Chem. Phys. 13 (18), 9141–9158.
Platt, S.M., El Haddad, I., Pieber, S.M., Zardini, A.A., Suarez-Bertoa, R., Clairotte, M., Daellenbach, K.R., Huang, R.J., Slowik, J.G., Hellebust, S., Temime-Roussel, B., Marchand, N., de Gouw, J., Jimenez, J.L., Hayes, P.L., Robinson, A.L., Baltensperger, U., Astorga, C., Prevot, A.S.H., 2017. Gasoline cars produce more carbonaceous particulate matter than modern filter-equipped diesel cars. Sci. Rep. 7 (4926), 1–9.
Shakya, K.M., Griffin, R.J., 2010. Secondary organic aerosol from photooxidation of polycyclic aromatic hydrocarbons. Environ. Sci. Technol. 44 (21), 8134–8139.
Shen, X., Yao, Z., Huo, H., He, K., Zhang, Y., Liu, H., Ye, Y., 2014. PM2.5 emissions from light-duty gasoline vehicles in Beijing. China. Sci. Total Environ. 487, 521–527.
Shorter, J.H., Herndon, S., Zahniser, M.S., Nelson, D.D., Wormhoudt, J., Demerjian, K.L., Kolb, C.E., 2005. Real-time measurements of nitrogen oxide emissions from in-use New York City transit buses using a chase vehicle. Environ. Sci. Technol. 39, 7991–8000.
Tong, H.Y., Hung, W.T., Cheung, C.S., 2000. On-road motor vehicle emissions and fuel consumption in urban driving conditions. J. Air & Waste Manage. Assoc. 50 (4), 543–554.
Wang, X.M., Sheng, G.Y., Fu, J.M., Chan, C.Y., Lee, S.C., Chan, L.Y., Wang, Z.S., 2002. Urban roadside aromatic hydrocarbons in three cities of the Pearl River Delta, People's Republic of China. Atmos. Environ. 36 (33), 5141–5148.
Wang, X., Westerdahl, D., Wu, Y., Pan, X.C., Zhang, K.M., 2011. On-road emission factor distributions of individual diesel vehicles in and around Beijing, China. Atmos. Environ. 45 (2), 503–513.
Wang, X., Yin, H., Ge, Y., Yu, L., Xu, Z., Yu, C., Shi, X., Liu, H., 2013. On-vehicle emission measurement of a light-duty diesel van at various speeds at high altitude. Atmos. Environ. 81, 263–269.
Wang, X., Liu, T., Bernard, F., Ding, X., Wen, S., Zhang, Y., Zhang, Z., He, Q., Lu, S., Chen, J., Saunders, S., Yu, J., 2014. Design and characterization of a smog chamber for studying gas-phase chemical mechanisms and aerosol formation. Atmos. Meas. Tech. 7 (1), 301–313.
Yang, W., Zhang, Q., Wang, J., Zhou, C., Zhang, Y., Pan, Z., 2018. Emission characteristics and ozone formation potentials of VOCs from gasoline passenger cars at different driving modes. Atmos. Pollut. Res. 9 (5), 804–813.
Yao, Z., Shen, X., Ye, Y., Cao, X., Jiang, X., Zhang, Y., He, K., 2015. On-road emission characteristics of VOCs from diesel trucks in Beijing, China. Atmos. Environ. 103, 87–93.
Yi, Z., Wang, X., Sheng, G., Zhang, D., Zhou, G., Fu, J., 2007. Soil uptake of carbonyl sulfide in subtropical forests with different successional stages in south China. J. Geophys. Res.-Atmos. 112, D08302. https://doi.org/10.1029/2006jd008048.
Zhang, Y., Wang, X., Blake, D.R., Li, L., Zhang, Z., Wang, S., Guo, H., Lee, F.S.C., Gao, B., Chan, L., Wu, D., Rowland, F.S., 2012. Aromatic hydrocarbons as ozone precursors before and after outbreak of the 2008 financial crisis in the Pearl River Delta region, south China. J. Geophys. Res.-Atmos. 117, D15306. https://doi.org/10.1029/2011jd017356.
Zhang, Y., Wang, X., Barletta, B., Simpson, I.J., Blake, D.R., Fu, X., Zhang, Z., He, Q., Liu, T., Zhao, X., Ding, X., 2013a. Source attributions of hazardous aromatic hydrocarbons in urban, suburban and rural areas in the Pearl River Delta (PRD) region. J. Hazard. Mater. 250, 403–411.
Zhang, Y., Wang, X., Zhang, Z., Lu, S., Shao, M., Lee, F.S.C., Yu, J., 2013b. Species profiles and normalized reactivity of volatile organic compounds from gasoline evaporation in China. Atmos. Environ. 79, 110–118.
Zhang, Y.L., Wang, X.M., Li, G.H., Yang, W.Q., Huang, Z.H., Zhang, Z., Huang, X.Y., Deng, W., Liu, T.Y., Huang, Z.Z., Zhang, Z.Y., 2015a. Emission factors of fine particles, carbonaceous aerosols and traces gases from road vehicles: recent tests in an urban tunnel in the Pearl River Delta, China. Atmos. Environ. 122, 876–884.
Zhang, Z., Wang, X.M., Zhang, Y.L., Lu, S.J., Huang, Z.H., Huang, X.Y., Wang, Y.S., 2015b. Ambient air benzene at background sites in China's most developed coastal regions: exposure levels, source implications and health risks. Sci. Total Environ. 511, 792–800.
Zhang, Y.L., Wang, X.M., Wen, S., Herrmann, H., Yang, W.Q., Huang, X.Y., Zhang, Z., Huang, Z.H., He, Q.F., George, C., 2016a. On-road vehicle emissions of glyoxal and methylglyoxal from tunnel tests in urban Guangzhou, China. Atmos. Environ. 127, 55–60.
Zhang, Z., Zhang, Y.L., Wang, X.M., Lu, S.J., Huang, Z.H., Huang, X.Y., Yang, W.Q., Wang, Y.S., Zhang, Q., 2016b. Spatiotemporal patterns and source implications of aromatic hydrocarbons at six rural sites across China's developed coastal regions. J. Geophys. Res.-Atmos. 121 (11), 6669–6687.
Zhang, Y., Yang, W., Simpson, I., Huang, X., Yu, J., Huang, Z., Wang, Z., Zhang, Z., Liu, D., Huang, Z., Wang, Y., Pei, C., Shao, M., Blake, D.R., Zheng, J., Huang, Z., Wang, X., 2018. Decadal changes in emissions of volatile organic compounds (VOCs) from on-road vehicles with intensified automobile pollution control: case study in a busy urban tunnel in South China. Environ. Pollut. 233, 806–819.
Zhao, Y., Hennigan, C.J., May, A.A., Tkacik, D.S., de Gouw, J.A., Gilman, J.B., Kuster, W.C., Borbon, A., Robinson, A.L., 2014a. Intermediate-volatility organic compounds: a large source of secondary organic aerosol. Environ. Sci. Technol. 48 (23), 13743–13750.
Zhao, Y., Hennigan, C.J., May, A.A., Tkacik, D.S., de Gouw, J.A., Gilman, J.B., Kuster, W.C., Borbon, A., Robinson, A.L., 2014b. Intermediate-volatility organic compounds: a large source of secondary organic aerosol. Environ. Sci. Technol. 48 (23), 13743–13750.
Zhao, Y., Nguyen, N.T., Presto, A.A., Hennigan, C.J., May, A.A., Robinson, A.L., 2015. Intermediate volatility organic compound emissions from on-road diesel vehicles: chemical composition, emission factors, and estimated secondary organic aerosol production. Environ. Sci. Technol. 49 (19), 11516–11526.
Zhao, Y., Nguyen, N.T., Presto, A.A., Hennigan, C.J., May, A.A., Robinson, A.L., 2016. Intermediate volatility organic compound emissions from on-road gasoline vehicles and small off-road gasoline engines. Environ. Sci. Technol. 50 (8), 4554–4563.